Thermally Induced Superstructure Stresses in Prestressed Girder Integral Abutment Bridges

Michael Paul, Jeffrey A. Laman, and Daniel G. Linzell

Forces and stresses that develop in the superstructure of prestressed concrete integral abutment bridges as a result of thermal load are investigated. Applied loading consists of uniform temperature changes in the superstructure. The influence of bridge length, number of spans, abutment height, and pile orientation on thermally induced superstructure forces is investigated. The largest thermally induced superstructure forces and stresses occurred near the abutment. It was determined that bridge length and abutment height most strongly influence thermally induced superstructure forces. The number of spans has the greatest influence on thermally induced superstructure stresses. Pile orientation influences thermally induced superstructure forces and stresses to a smaller degree. Results also indicate that thermally induced superstructure stresses and shear forces are comparable in magnitude to those caused by live load.

Integral abutment (IA) bridges have two major advantages over traditional jointed bridges: the expansion joints are eliminated, which can reduce construction and maintenance costs (*1, 2*), and the rigidity of the superstructure–abutment connection provides additional redundancy to the structure. A major drawback of IA bridges is undesirable thermally induced stresses that develop in girders, deck slabs, abutments, and piles. It has been suspected that thermally induced stresses in IA bridge structural components can approach those due to gravity load stresses. This study investigates the influence of thermal loads on IA bridge component stresses relative to gravity load stresses through a limited parametric study that includes bridge length, number of spans, abutment height, and pile orientation. Selected parameter ranges (Table 1) are based on normal ranges used for current IA bridge construction. The IA bridge type considered for this study is concrete slab on four prestressed concrete girders. The study objectives are to establish an accurate numerical modeling procedure, determine the degree of parameter influence, and determine superstructure locations exhibiting the most detrimental thermally induced stresses.

To design the numerical parametric study and accurately evaluate the influence of thermal loading on IA bridges, preliminary numerical studies were conducted to evaluate (*a*) the level of analysis required for the parametric study and (*b*) suitable member connectivity stiffness between the abutment and girders. This preliminary evaluation was conducted through a comparison of numerical results to field data collected from an IA bridge in central Pennsylvania. In addition, available literature was reviewed to establish (*a*) a suitable numerical modeling technique for soil–structure interaction, (*b*) accepted thermal expansion coefficients for concrete, (*c*) normal design temperature range, and (*d*) models of temperature gradient.

It was the desire of the research team to design the most extensive parametric study possible given limited resources; therefore, a simplified 2-D model was considered. To justify a 2-D simplified model as the level of analysis, 2-D simplified and 3-D FEM models of the tested central Pennsylvania bridge were developed and responses (i.e., deformations and stresses) compared. On the basis of this comparison, a suitable model was selected. In addition to level of analysis, methods for modeling of the backwall to abutment joint were investigated through numerical analysis and field measurements.

Soil–structure interaction modeling significantly influences the response of an IA bridge. Soil density, internal friction angle, soil-to-wall friction, wing-wall orientation, and backfill angle can all influence the interaction. Methods used to model soil pressures range from neglecting all soil pressures (*2*), to simplified assumptions of passive and active pressures during thermal expansion and contraction of the bridge, respectively, to more sophisticated, nonlinear modeling or iterative procedures (*3*). To most accurately model the effect of soil pressure on the abutment and piles, a multilinear spring based on fundamental *p-y* (load–displacement) soil behavior was used.

Concrete is a composite material with a thermal expansion coefficient dependent on constituent material properties, concrete age, and environmental factors (*4*). Emanuel and Hulsey (*5*) listed seven factors other than stress that affect volume change for concrete: (*a*) richness of mix, (*b*) cement type, (*c*) aggregate type, (*d*) water–cement ratio, (*e*) age, (*f*) temperature, and (*g*) alternations of high and low temperature. The concrete thermal expansion coefficient recommended for design by AASHTO is 6.0×10^{-6} in./in./°F. However, a study by Ndon and Bergeson (*4*) measured thermal coefficients of two concrete girder IA bridges in Iowa over a 3-year period. Calculated expansion coefficients ranged between 4.0×10^{-6} in./in./°F and 4.7×10^{-6} in./in./°F. Concrete core samples were taken from these two bridges with laboratory results ranging between 4.5×10^{-6} in./in./°F and 5.2×10^{-6} in./in./°F. On the basis of the literature, an average expansion coefficient magnitude of 5.0×10^{-6} in./in./°F was used for numerical models in this study.

M. Paul, Wilbur Smith Associates, 5555 Hilton Avenue, Suite 325, Baton Rouge, LA 70808. J. A. Laman, 231J Sackett Building, and D. G. Linzell, 231L Sackett Building, Pennsylvania State University, University Park, PA 16802.

Transportation Research Record: Journal of the Transportation Research Board, CD 11-S, Transportation Research Board of the National Academies, Washington, D.C., 2005, pp. 287–297.

TABLE 1 Varied Bridge Parameters

Bridge Length, m (ft) (1)	Number of Spans (2)	Abutment Height, m (ft) (3)	Steel H-Pile Orientation (4)
46.3 (152)	1, 2	1.2 (4), 2.7 (9), 4.3 (14)	Strong (OS) and Weak (OW)
105.0 (345)	3, 4		
183.0 (600)	4, 5		
244.0 (800)	5, 6		
305.0 (1000)	6, 7, 8		

The effects of temperature differentials or gradients caused by solar radiation, precipitation, wind velocity, and thermal mass in a structure are often neglected in design, and a uniform temperature distribution is assumed for simplicity. Temperature gradients in the transverse and longitudinal directions of a bridge tend to be fairly constant (*4*); however, the greatest variation in temperature occurs through the bridge depth. Figure 1 shows positive and negative temperature gradients through the depth of a superstructure (*6*). The effects of a temperature gradient versus uniform temperature changes were evaluated as part of the preliminary study. On the basis of this study, it was determined that the gradient effect was not significant relative to other parameters; therefore, a constant superstructure temperature load was applied through the cross section.

Following the completion of the preliminary studies described above, the parametric study was designed and conducted to evaluate levels of force and stress induced in the various bridge configurations under thermal loading. Evaluated responses are girder bending moment, shear force, and axial force; bottom-of-beam stress and top-of-slab stress are presented in the discussion section of this paper.

MONITORED INTEGRAL ABUTMENT BRIDGE

Bridge 203 was used for comparison with both 2-D and 3-D numerical results. The bridge, which is located on I-99 in central Pennsylvania, carries two lanes of traffic over US-322. Out-to-out width is 13.1 m (42.9 ft), with three spans of length 14.3 m (47.0 ft), 26.8 m (88.0 ft), and 11.3 m (37.0 ft). The bridge is a four-girder, prestressed concrete slab-on-beam structure. Both piers support girders through elastomeric bearings. Abutment 1 (south end) is a fixed abutment that is cast against rock. Abutment 2 (north end) is a 4.4-m (14.3-ft) tall integral abutment that bears on a row of eight HP 12 × 74 end-bearing piles oriented for weak axis bending.

This bridge has been extensively instrumented to monitor movements at several locations in the substructure along with strains in the girders. Extensometers were installed behind Abutment 2 to measure longitudinal translations and inferred rotations about a vertical and transverse axis. Strain gauges are located at the top and bottom of each of the four girders at midspan and at the abutment for Span 3. The bridge has been monitored for 8 months, with detailed monitoring results presented elsewhere (*7*).

NUMERICAL MODELING

Preliminary Study Discussion

To evaluate the accuracy of a 2-D simplified model as compared with a 3-D FEM model for the purposes of the present parametric study, a preliminary study was conducted to compare the response of the monitored central Pennsylvania bridge with the numerical 2-D and 3-D models' response. Representations of each of the models are shown in Figure 2*a* and 2*b,* respectively. STAAD Pro Release 2002 was used for all numerical analyses in the present study, and the 2-D and 3-D models were developed with the same boundary conditions, member connectivity, and soil-modeling techniques.

A number of key modeling details were important to the preliminary study and accurate modeling of the bridge. Of critical interest was the connection of the girders and abutment diaphragm to the abutment. The actual superstructure is connected to the abutment by means of the abutment diaphragm as shown in Figure 3. This preliminary study considered released, full, and partial *z*-axis rotational restraint and full and partial *x*-direction translational restraint (relative to the axes system in Figure 3) at the joint. Rotational restraint was determined by means of a moment–curvature relationship developed on the basis of basic mechanics principles and the actual construction detail (*8*). The standard Pennsylvania Department of Transportation connection detail specifies connection joint reinforcement that offers significantly less bending capacity but higher ductility than the corresponding abutment reinforcement. An elastic–plastic relationship was assumed for the moment–rotation relationship, in which the linear *z*-axis rotational stiffness, K_r, is effective until the yield moment, M_y, and corresponding rotation, θ_y, are reached. At the point of yielding, a hinge is formed, and it was assumed that the connection joint offered no additional bending resistance. An *x*-direction translational spring was also modeled at the location of the connection joint. Translational spring stiffness between the abutment diaphragm and the abutment was determined by using basic mechanics principles and incorporated in the models.

Both 2-D and 3-D models considered abutment and pile passive soil pressure as a nonlinear response (*9, 10*), using a multilinear

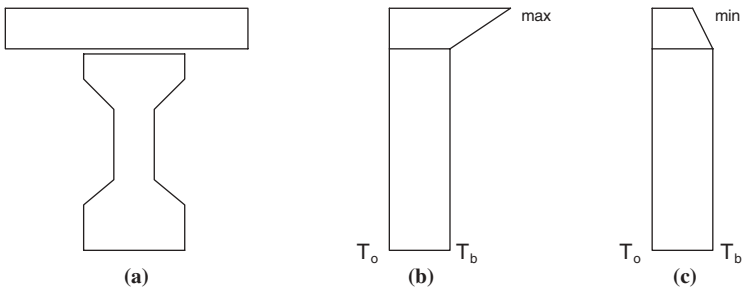

FIGURE 1 Temperature gradients considered (*6*): (*a*) bridge section, (*b*) positive gradient, and (*c*) negative gradient (T_o = casting temperature and T_b = seasonal temperature).

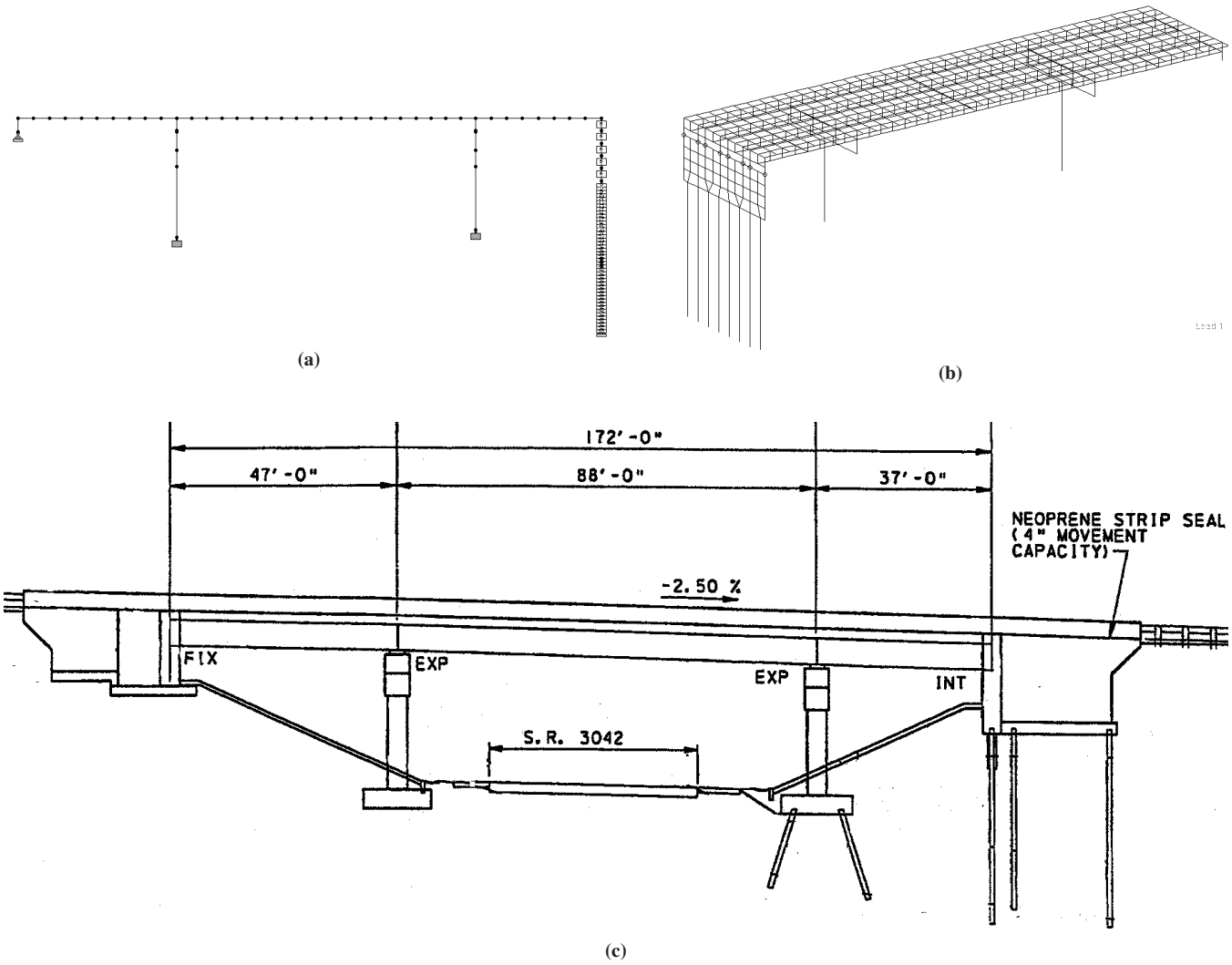

FIGURE 2 Numerical models and Bridge 203: (*a*) 2-D numerical model of Bridge 203, (*b*) 3-D numerical model of Bridge 203, and (*c*) Bridge 203 elevation.

approximation to model the passive soil pressures (*3*). Abutments and piles were discretized, and multilinear springs were modeled to simulate passive soil pressure in the 2-D and 3-D models. A triangular pressure distribution was assumed for modeling the active abutment soil forces for bridge contraction. STAAD offers a multilinear spring support element that is critical to the modeling of nonlinear soil behavior at the substructure. The multilinear spring support element provides a convenient method to approximate nonlinear passive and active soil response that occurs at piles and abutments (*3*).

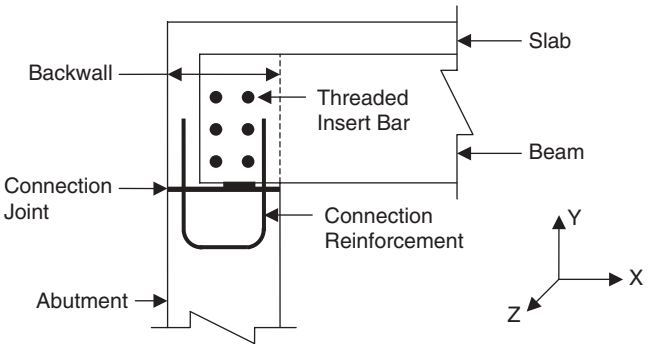

FIGURE 3 Typical abutment to superstructure connection detail.

Uniform temperature loads of +26.7°C (+80°F) and −26.7°C (−80°F) were applied to the superstructure in the models based on the *AASHTO LRFD Bridge Design Specifications* (*11*). Live load stresses were calculated on the basis of the standard HL93 truck model, considering number of lanes and multiple presence, for comparison with thermal load stresses.

Preliminary Study Discussion of Results

Along with the incorporation of the previously discussed rotational and translational springs, numerical 2-D and 3-D modeling cases incorporating fixed and pinned superstructure to abutment connections were considered as the extreme of superstructure to abutment connectivity. These cases are designated in Figures 4 and 5 as "pinned conn" and "fixed conn," modeling the connection joint with *z*-axis rotation connectivity released and fixed, respectively. The "R spring"

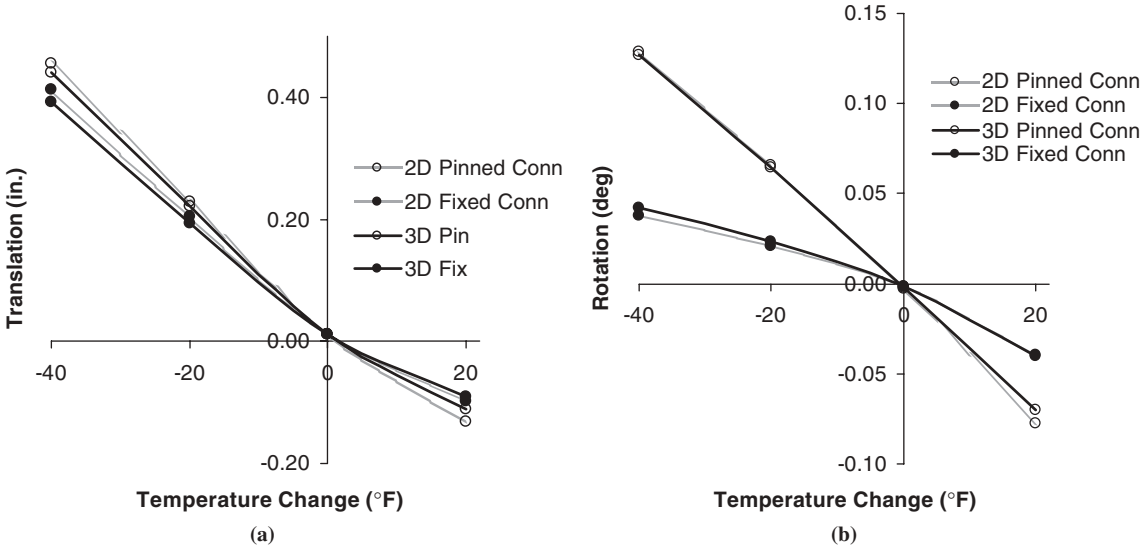

FIGURE 4 Comparison of (*a*) 2-D versus 3-D abutment translation and (*b*) 2-D versus 3-D abutment rotation.

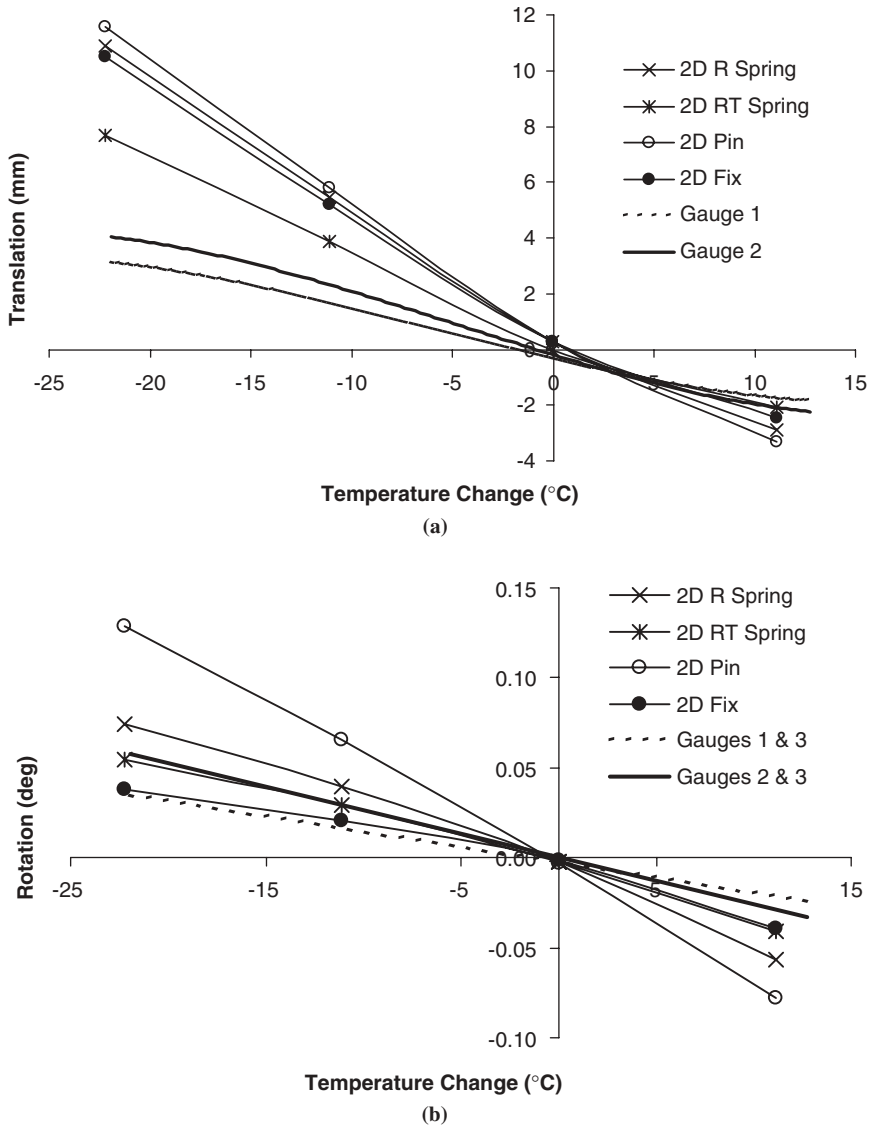

FIGURE 5 Influence of temperature on abutment movements: (*a*) deflection and (*b*) rotation.

case models the *z*-axis rotational spring at the connection joint, and the "RT spring" case models the *z*-axis rotational spring combined with an *x*-direction translational spring at the connection joint.

Figures 4*a* and 4*b* present 2-D and 3-D model response results for abutment translation and rotation considering fixed and pinned conditions. Very little difference in response was observed between the two models for both the fixed and pinned cases. As a result, the 2-D model was the focus of further evaluation as compared with the field response.

A translational spring modeled at the connection joint was the most influential parameter in matching the numerical response to the field response. The translational spring is capable of accounting for both relative movement between the superstructure and abutments and other secondary effects such as creep. Presented in Figure 5*a* and 5*b* is a representative comparison between field data and 2-D numerical model abutment rotation and translation. Two extensometers located at the top of the abutment are designated as Gauges 1 and 2, and a third extensometer at a lower elevation, when combined with Gauges 1 and 2, allows for the calculation of abutment rotation. Results presented for the gauge data are a third-order best fit of extensive field monitoring data. It can be seen from Figure 5*b* that the rotational fixity at the connection joint has little influence on the top of abutment rotation, which indicates that lack of abutment movement would need to be accounted for.

Figure 6 shows a comparison of bottom-of-beam stress. Third-order best fit curves are shown for the stresses that were calculated from the measured strains of the beams.

On the basis of the above preliminary study, the 2-D numerical model that includes both a rotational and translational spring at the girder-to-abutment connection was used to conduct the parametric study.

PARAMETRIC STUDY RESULTS

The thermally induced superstructure expansion and contraction [±26.7°C (±80°F)] causes soil pressure to be applied to the abutments and piles, which causes moments and axial and shear forces in the superstructure at the location of the abutments. However, there is little thermally induced moment or axial force at the piers, because of low rotation and longitudinal restraint at the pier bearing. Figure 7 shows bending, axial force, and shear force diagrams from the 2-D models for bridge expansion and contraction resulting from thermal loading. The cases are shown for a 6-span, 305-m (1,000-ft) bridge length with piles oriented to bend about the strong axis for three different abutment heights (H1.2, H2.7, H4.3), designated as 305-S6-OS-H1.2-E, 305-S6-OS-H2.7-E, 305-S6-OS-H4.3-E, and so on. The coding for bridge configuration in the parametric study for Illustrative Case 305-S6-OS-H1.2-E is as follows:

- 305 refers to total bridge length, in meters;
- S6 refers to number of spans in the total length;
- OS refers to H-pile orientation: OS = oriented strong and OW = oriented weak;
- H1.2 refers to the abutment height measured from underside of girder to top of pile; and
- E refers to temperature sign: E = expansion and C = contraction.

The largest superstructure moments occur at the abutment, axial forces are constant across the length of the bridge, and the shear force is constant across the length of each span.

Figure 7 also indicates the influence of abutment height. For bridge expansion, taller abutments cause larger thermally induced superstructure forces. Taller abutments have a larger area that is exposed to passive soil pressure, which results in larger forces. For bridge contraction, taller abutments cause smaller thermally induced superstructure forces because larger active soil forces act to oppose the passive pile soil force.

Shown in Figure 8*a* and 8*b* are 2-D model superstructure axial force and moment, respectively, for a range of bridge lengths. Superstructure forces shown are those that occur at the abutment, and bridges with similar span lengths were used for the comparison. It can be observed that thermally induced superstructure force increases as bridge length increases for both expansion and contraction, but the increase in force is not linear. Bridge lengths beyond approximately 100 m (328 ft) do not experience a significant increase in axial force, and lengths beyond approximately 180 m (590 ft) do not experience a significant increase in moment, largely because of the nonlinear abutment and pile soil response.

Figure 9 shows axial, top-of-slab, and bottom-of-beam bending stresses and combined axial and bending stresses for the 305-S6-OS-H1.2-E case. It can be seen that bending and axial girder stresses follow the same trends as the respective forces. The largest magnitude of thermally induced stress always occurs in the bottom of the beams at the location of the abutment. For bridge expansion, the negative moment at the abutment and the compressive bridge axial force combine to create a relatively large normal compressive stress in the bottom of the beams at this location. For bridge contraction the positive moment at the abutment and tensile bridge axial force create the relatively large normal tensile stresses at this location. Thermally induced superstructure bending stresses decrease in magnitude near the center of the bridge. At interior span locations the axial component of stress makes the largest contribution to the level of thermally induced normal stress.

Abutment height and bridge length may have a large influence on superstructure force; however, span configuration has the largest influence on bridge stress. Typically, bridges with a larger number of spans (shorter span lengths) will experience larger top-of-slab and bottom-of-beam thermally induced stresses. Longer span lengths tend to be stiffer, which results in a larger section modulus (I/y). The smaller section moduli for shorter spans result in larger thermally induced superstructure stresses. Table 2 shows bending stress comparisons for the 105-S3-OS-H1.2, 105-S4-OS-H1.2, 305-S6-OS-H1.2, and 305-S8-OS-H1.2 cases. Stresses are presented for the top-of-slab and bottom-of-beam locations at the abutment and each pier. Larger stresses occur for the 105-S4-OS-H1.2 and 305-S8-OS-H1.2 cases. The table also demonstrates that it is possible for a bridge with longer spans to exhibit smaller thermally induced stresses than a bridge with shorter spans.

The studies also showed that piles oriented to bend about the strong axis cause larger thermally induced superstructure forces and stresses than piles oriented to bend about their weak axis. Pile orientation has the least amount of influence on superstructure stress; the pile orientation caused changes in superstructure stress that were usually less than 7%.

Live load stresses and shear force were compared with those caused by thermal movements. Figure 10 is a representative comparison for the 305-S6-OS-H1.2 case. Bridge expansion causes large compressive stress in the bottom of the beams and large tensile stress in the top of the slab at the abutment, which would cause detrimental effects when superimposed with live load moment at this location. However, because of the relatively low strength capacity

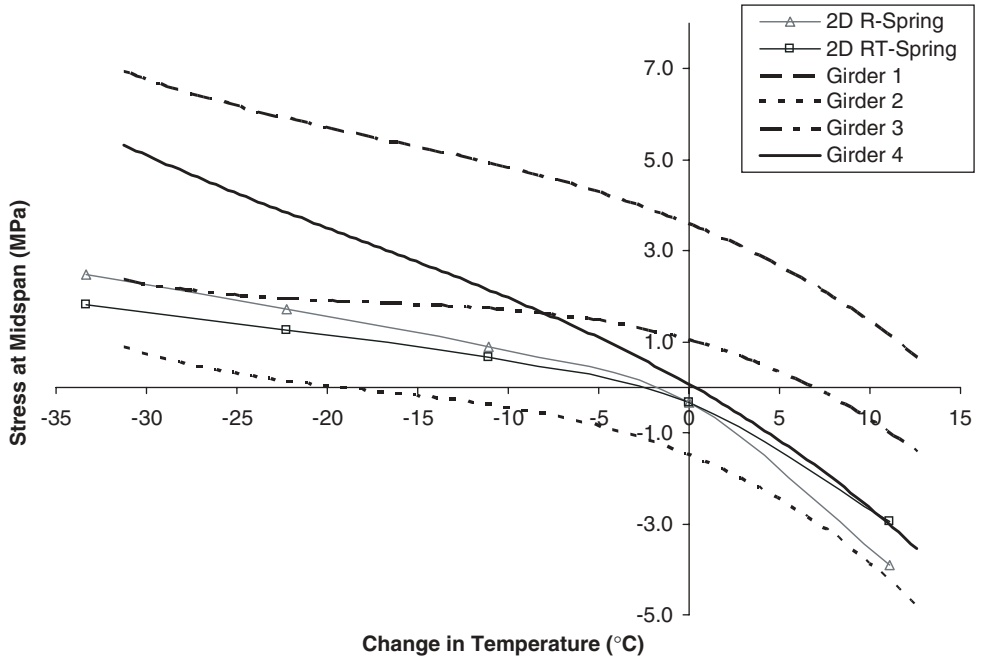

(a)

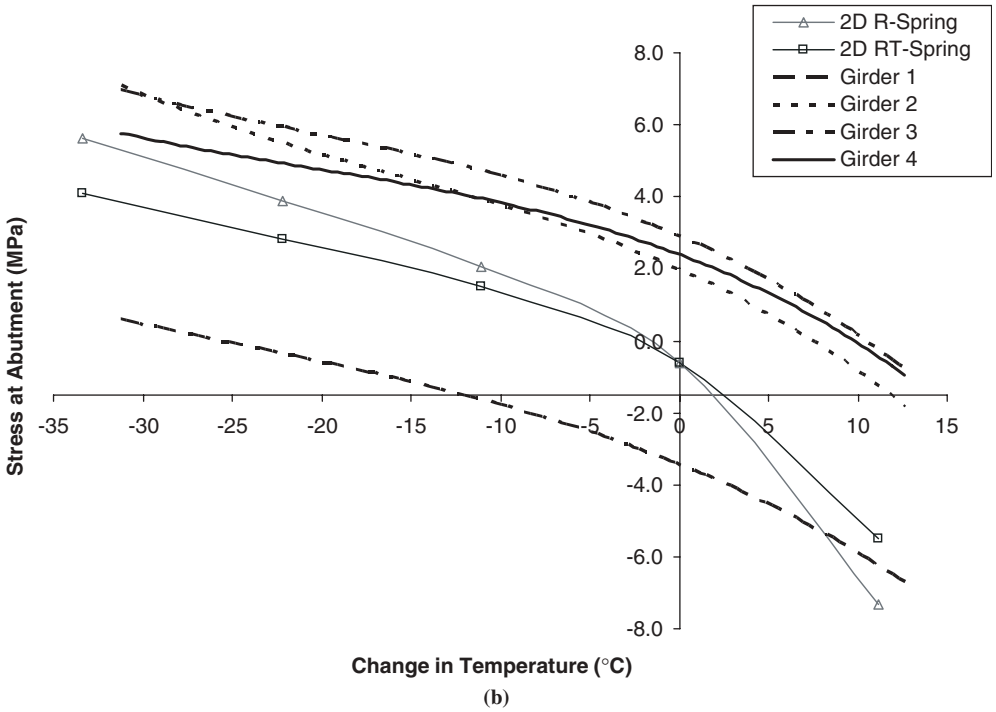

(b)

FIGURE 6 Bottom-of-beam stress at (*a*) midspan and (*b*) abutment.

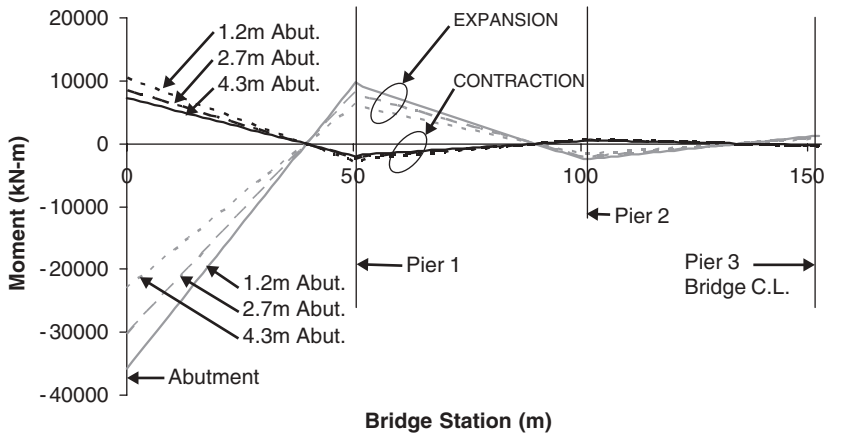

(a)

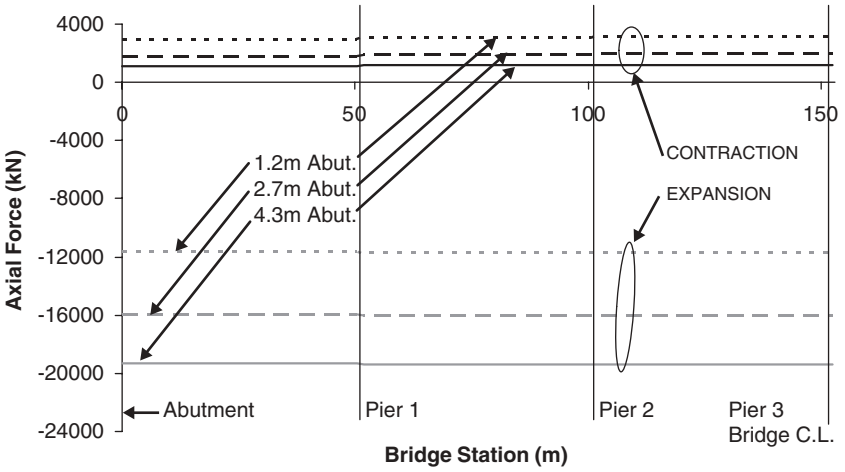

(b)

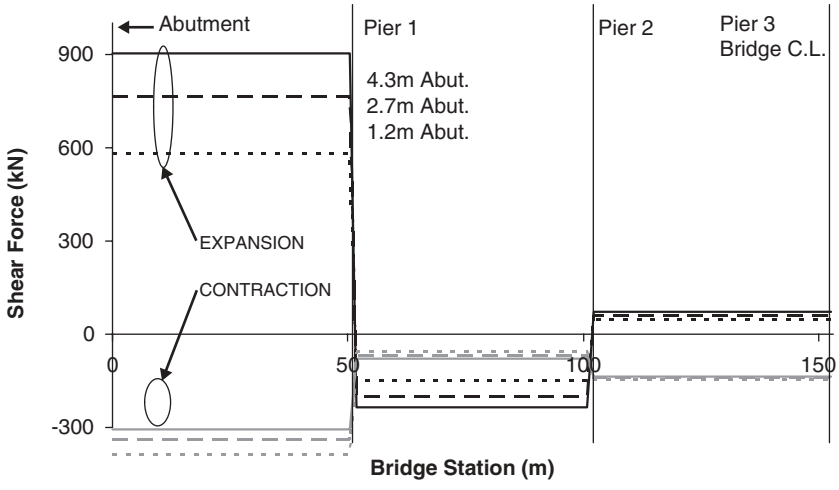

(c)

FIGURE 7 Thermally induced superstructure forces for 305-m bridge: (*a*) bending moment, (*b*) axial force, and (*c*) shear force.

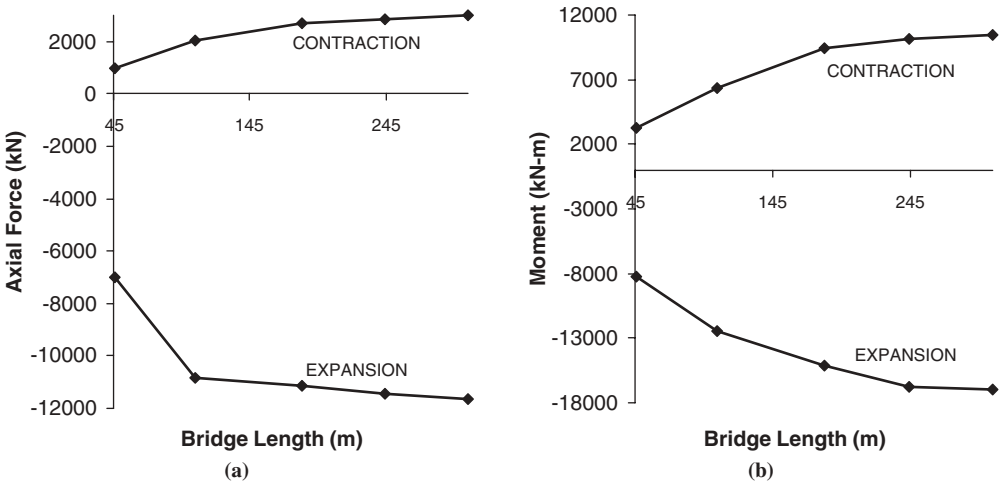

FIGURE 8 Thermally induced forces as a function of bridge length: (*a*) axial force and (*b*) moment.

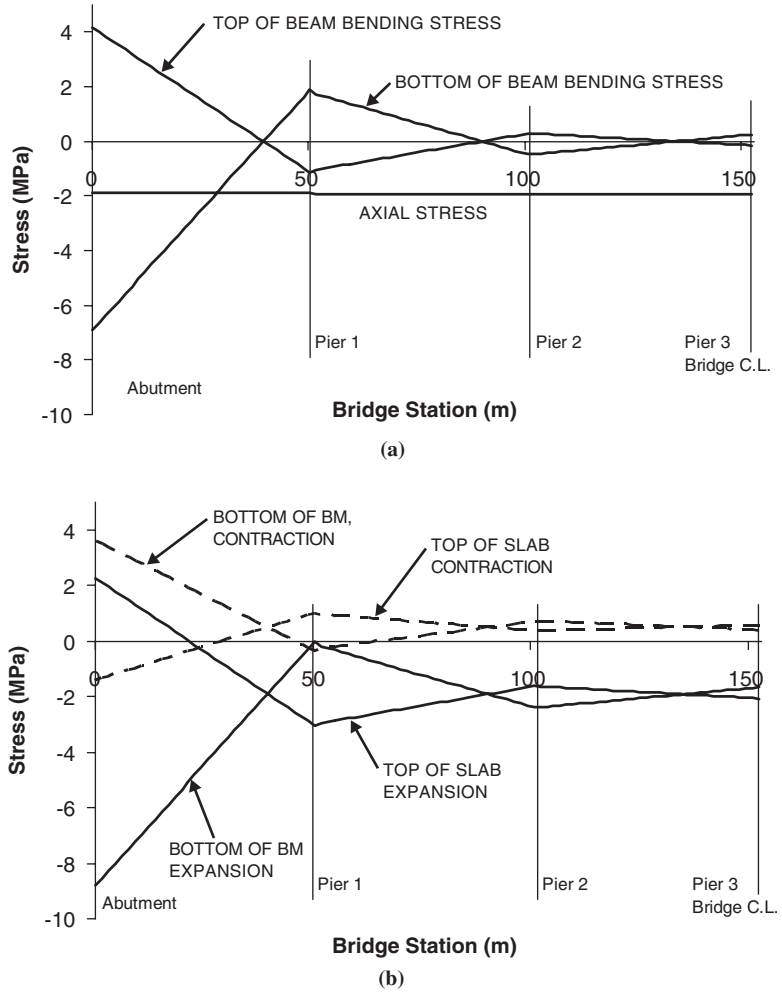

FIGURE 9 Thermally induced superstructure stresses for 305-m bridge: (*a*) components of stress and (*b*) total thermal stress.

TABLE 2 Superstructure Stress

Bridge Geometry* (1)	Stress Location (2)	Bottom Stress** MPa (ksi) (3)	Top Stress** MPa (ksi) (4)
105-S3-OS-H1.2-E	Abutment	-11.34 (-1.64)	3.30 (0.49)
	Pier 1	-0.45 (-0.06)	-3.08 (-0.45)
105-S3-OS-H1.2-C	Abutment	3.89 (0.55)	-1.64 (-0.24)
	Pier 1	-0.08 (-0.01)	1.30 (0.19)
105-S4-OS-H1.2-E	Abutment	-13.77 (-2.00)	4.27 (0.62)
	Pier 1	0.74 (0.11)	-4.14 (-0.60)
	Pier 2	-3.73 (-0.54)	-1.78 (-0.26)
105-S4-OS-H1.2-C	Abutment	4.90 (0.71)	-2.16 (-0.31)
	Pier 1	-0.72 (-0.10)	-1.15 (-0.17)
	Pier 2	0.92 (0.13)	0.35 (0.05)
305-S6-OS-H1.2-E	Abutment	-8.81 (-1.28)	2.25 (0.33)
	Pier 1	-0.05 (-0.01)	-2.96 (-0.43)
	Pier 2	-2.41 (-0.35)	-1.63 (-0.24)
	Pier 3	-1.67 (-0.24)	-2.05 (-0.30)
305-S6-OS-H1.2-C	Abutment	3.62 (0.53)	-1.39 (-0.20)
	Pier 1	0.34 (0.05)	0.96 (0.14)
	Pier 2	0.72 (0.10)	0.37 (0.54)
	Pier 3	0.39 (0.06)	0.57 (0.08)
305-S8-OS-H1.2-E	Abutment	-12.48 (-1.81)	3.23 (0.49)
	Pier 1	0.13 (0.02)	-3.46 (-0.50)
	Pier 2	-3.23 (-0.47)	-1.79 (-0.26)
	Pier 3	-2.37 (-0.34)	-2.22 (-0.32)
	Pier 4	-2.64 (-0.38)	-2.09 (-0.30)
305-S8-OS-H1.2-C	Abutment	5.40 (0.78)	-2.00 (-0.29)
	Pier 1	-0.60 (-0.09)	1.19 (0.17)
	Pier 2	0.99 (0.14)	0.41 (0.06)
	Pier 3	0.59 (0.09)	0.62 (0.09)
	Pier 4	0.73 (0.11)	0.56 (0.08)

* See section on parametric study results for coding explanation.
** + = tension, - = compression.

of the connection joint, the live load moment induced into the superstructure at this location will not exceed the joint yield moment. For longer length bridges that have undergone large enough thermal movements to cause yielding of the connection joint, superimposed live load will not cause any additional negative moment. The situation for the thermally induced shear force is similar to that for thermally induced stress. Gravity loads cause relatively large shear forces in the superstructure at the abutments. However, once the bending capacity of the connection joint is exceeded, thermal movement will not cause any additional shear force in the superstructure.

Bridge thermal movements cause relatively low bottom-of-beam stresses at the first interior pier (Figure 7). However, thermal movements cause relatively large top-of-slab stresses at this location. Bridge expansion causes compression in the top of the slab, and bridge contraction causes tension. Bridge contraction is the more detrimental case because live load also causes tension in the slab. When bridge contraction and live load are superimposed, tensile cracking in the slab may occur. The tensile strength of the slab is about 3.24 MPa (0.47 ksi); the thermally induced stress at this location is usually between +0.69 MPa (+0.1 ksi) and +1.38 MPa (+0.2 ksi) in the studied bridges, and live load stresses are approximately the same as or less than the thermally induced stress.

At each of the successive pier locations, the bending stress is relatively small when compared with axial stress, and this axial stress makes up the largest portion of the top-of-slab and bottom-of-beam stresses. At these locations, bridge expansion causes compressive stress in the superstructure and bridge contraction tensile stress. Bridge expansion will have undesirable effects on the bottom of the beam when superimposed with live load stresses because relatively large compressive stresses can result. At this location these compressive stresses will most likely not cause damage because compressive stresses are less than 6.9 MPa (1 ksi) for each studied bridge case. Bridge contraction will have undesirable effects on the top of slab when superimposed with live load stresses because both loads cause tension which, again, could potentially cause cracking of the slab. Thermally induced stresses at these locations are large relative to the total stress level, being 1.03 MPa (0.15 ksi) or less, which is approximately 30% of the concrete slab tensile strength.

Thermally induced superstructure shear forces at the piers also have the potential to combine with the dead load and live load shear forces. It is only at the first pier location that significant thermally induced shear forces occur (Figure 7). At this location bridge contraction causes shear stresses that can combine with gravity load shear forces to cause potentially damaging effects.

Thermally induced shear stresses at midspan can produce detrimental effects, particularly at the end span and adjacent span. Gravity load shear forces are relatively small near midspan, but thermally induced shear forces are constant along the length of each span. Typically, in the end spans, thermally induced shear forces are equal to or greater than live load shear forces (see Figure 10). Typically, at Span 2 thermally induced shear forces are less than live load shear forces, but are not insignificant. That may result in shear reinforcement being underdesigned at these midspan locations.

CONCLUSIONS

As compared with normal design levels, thermal loads in the superstructure of the IA bridges studied herein caused significant magnitudes of bending and axial and shear forces in the superstructure. Bending and shear forces are largest near the abutments, and axial forces are constant across the length of the bridges that were examined. Generally, longer bridge lengths cause larger thermally induced superstructure forces. However, span length has a higher influence for thermally induced superstructure stress where shorter span lengths have larger thermally induced stress. Bridge expansion causes larger superstructure forces and stresses than bridge contraction; however, bridge contraction induces concrete tension and, therefore, may be more detrimental when superimposed with live load. Typically, taller abutments cause larger stresses for bridge expansion, but smaller stresses for bridge contraction. Live load induced moments in the superstructure do not cause any additional moments in the girder ends after the flexural capacity of the connection joint is exceeded. Typically, however, calculated thermally induced stresses exceeded the tensile strength of the beam and slab concrete at the abutment, which implies that cracking of the concrete may occur at this location. At the location of the end span and pier, relatively large tensile stresses in the bottom of the beams at midspan and at the top of the slab at the pier resulted from bridge contraction. That has undesirable effects when superimposed with gravity loads because the additional tensile stresses at these locations may produce cracking. At the location of the interior spans and piers, bridge expansion causes compression through the entire superstructure; the values are usually between 2.1 MPa (0.3 ksi) and 4.1 MPa (0.6 ksi). At these locations, bridge contraction causes tension through the entire superstructure; the values are usually between 0.34 MPa (0.05 ksi) and 1.03 MPa (0.15 ksi).

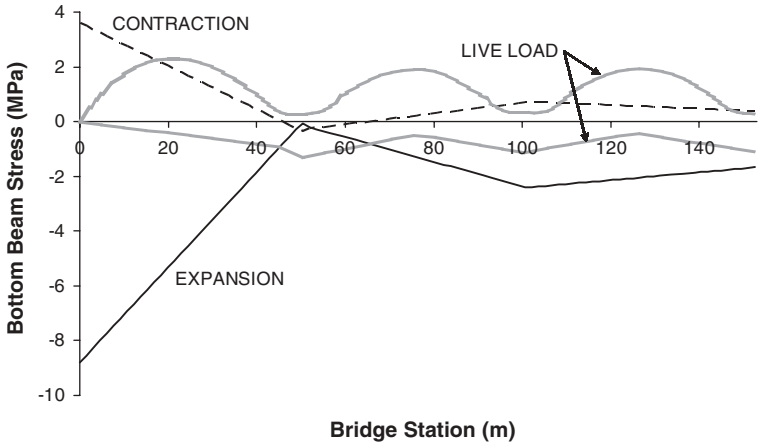

(a)

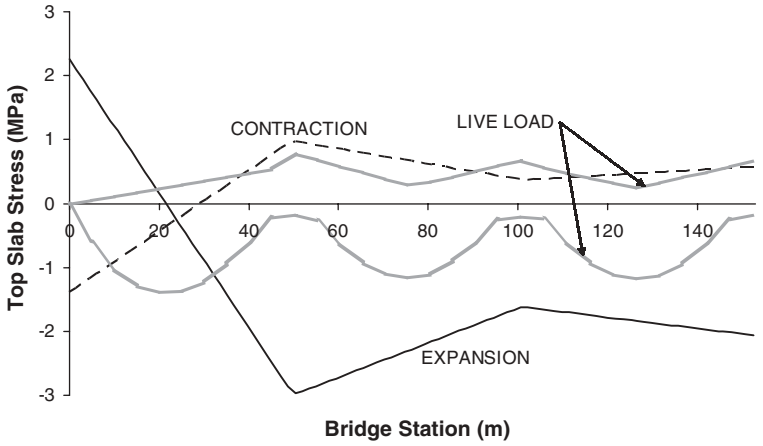

(b)

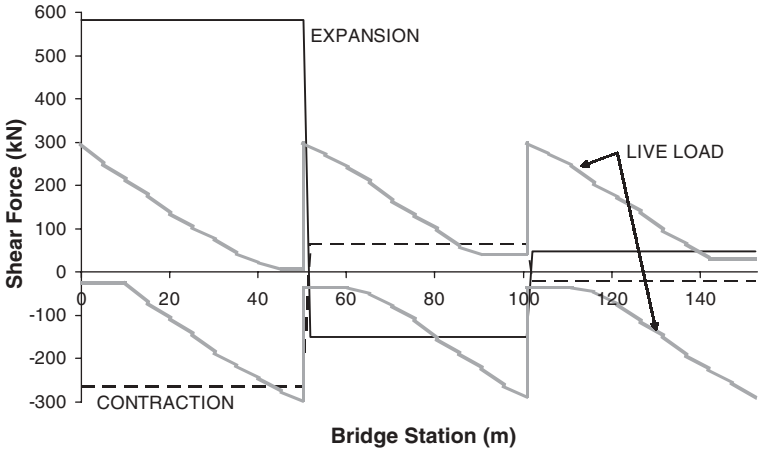

(c)

FIGURE 10 Live load and thermal stresses for 305-m bridge with 1.2-m abutment height: (*a*) beam bottom, (*b*) slab top, and (*c*) shear force.

REFERENCES

1. Soltani, A. A., and A. R. Kukreti. Performance Evaluation of Integral Abutment Bridges. In *Transportation Research Record 1371,* TRB, National Research Council, Washington, D.C., 1992, pp. 17–25.
2. Kunin, J., and S. Alampalli. Integral Abutment Bridges: Current Practices in the United States and Canada. *Journal of Performance of Constructed Facilities,* Vol. 14, No. 3, Aug. 2000, pp. 104–111.
3. Fennema, J. *Prediction of Integral Abutment Bridge Behavior.* M.S. thesis. Pennsylvania State University, University Park, 2003.
4. Ndon, U. J., and K. L. Bergeson. Thermal Expansion of Concretes: Case Study in Iowa. *Journal of Materials in Civil Engineering,* Vol. 7, No. 4, Nov. 1995, pp. 246–251.
5. Emanuel, J. H., and J. L. Hulsey. Prediction of the Thermal Coefficient of Expansion of Concrete. *ACI Journal,* Vol. 74, No. 4, April 1977, pp. 149–155.
6. Kennedy, J. B., and M. H. Soliman. Temperature Distribution in Composite Bridges. *Journal of Structural Engineering,* Vol. 113, No. 3, 1987, pp. 475–482.
7. Laman, J. A., D. G. Linzell, C. A. Leighty III, and J. L. Fennema. *Methodology to Predict Movement and Stresses in Integral Abutment Bridges*. University-Based Research, Education and Technology Transfer Program. Agreement No. 359704, Work Order 80. Final Report. Pennsylvania Department of Transportation, Harrisburg, March 2003.
8. Paul, M. D. *Thermally Induced Superstructure Stress in Prestressed Girder Integral Abutment Bridges.* M.S. thesis. Pennsylvania State University, University Park, 2003.
9. Reese, L. C., and W. Van Impe. Single Piles and Pile Groups Under Lateral Loading. *Applied Mechanics Reviews,* Vol. 55, No. 1, Jan. 2002, pp. B9–B10.
10. Koskinen, M. *Soil Structure Interaction of Jointless Bridges on Piles.* Geotechnical Laboratory, Tampere University of Technology, Finland, pp. 1091–1096.
11. *AASHTO LRFD Bridge Design Specifications,* 2nd ed. AASHTO, Washington, D.C., 1998.

The 6th International Bridge Engineering Conference Committee sponsored publication of this paper.